International Journal of Heat and Mass Transfer 234 (2024) 126138

Contents lists available at ScienceDirect

International Journal of Heat and Mass Transfer

journal homepage: www.elsevier.com/locate/ijhmt

A simple two-phase approach to predict moisture-dependent thermal conductivity for porous materials

C.H. Koh *, H.J.H. Brouwers

Department of the Built Environment, Eindhoven University of Technology, P. O. Box 513, 5600 MB Eindhoven, the Netherlands

ARTICLE INFO

Keywords:
Porous medium
Moisture
Thermal conductivity
Insulation
Multiphase Model

ABSTRACT

This study develops a generalized solution for moisture-dependent thermal conductivity (λ_{eff}) in porous media, utilizing readily available parameters. By introducing arbitrary dry and saturated phases, the tri-phase model (solid, gas, and water) is simplified into a two-phase model. Seven analytical solutions are adapted, including series-parallel, Maxwell-Eucken, Landauer's, exponential, and Somerton's relations. The proposed method requires only two parameters to predict λ_{eff} under different degrees of saturation (S_r): effective dry thermal conductivity (λ_{dry}, where $S_r = 0$) and effective saturated thermal conductivity (λ_{sat}, where $S_r = 1$). In the absence of direct λ_{sat} measurement, this λ_{sat} can be obtained using λ_{dry} and the parallel relation for highly porous media, and using Landauer's relation for medium-density materials. Validation results indicate that both Landauer's and exponential relations provide the upper bound and lower bounds, respectively, for λ_{eff}. For medium-density materials, the upper bound aligns with the parallel relation and the lower bound aligns with Landauer's relation.

1. Introduction

Building thermal insulation materials, and many mineral-based construction materials, commonly feature a porous structure to leverage the low thermal conductivity of air or gas within their pores. However, these porous materials are highly susceptible to moisture adsorption, condensation, rain, and groundwater uptake. The presence of water within the insulation materials introduces an additional thermal conductor, leading to increased heat transfer through the material. This rise in water content compromises the thermal resistance of the insulation material, thereby diminishing its performance. Despite efforts to mitigate moisture adsorption and water infiltration, complete avoidance is often challenging. Therefore, understanding how changes in water content impact the effective thermal conductivity of porous materials is essential.

Several methods are available for measuring the effective thermal conductivity of wet porous building materials. These methods include the transient method (periodic method) proposed by ISO 16957 [1], and the steady-state method using a standardized guarded hot plate or heat flow meter as outlined in ISO 10051 [2]. However, measuring the thermal conductivity of moist porous materials presents challenges. In the steady-state method, the applied temperature gradient induces a non-uniform distribution of moisture within the material. While this issue could potentially be addressed using the periodic method outlined in ISO 16957, this approach entails a more complex measurement setup and analysis. Consequently, a simple analytical solution based on commonly measured parameters, such as thermal conductivity under dry conditions, would prove advantageous in this context.

Material-specific approximation through data fitting is the simplest method. For example, McFadden [3] proposed simple linear and exponential relations for moist insulation material based on measurements using different techniques. However, for a generalized model, a more complex approach is required.

Wang et al. [4] applied a tri-phase thermal conductivity model based on capillary structure using fractal theory. This model considers parameters such as porosity, pore size distribution, and fractal structure in determining the thermal conductivity under different moisture content. Similarly, Qin et al. [5] applied a fractal model for porous media under different degrees of saturation. Pei et al. [6] introduced a tortuosity correction in their tri-phase model to reflect the heat conduction path, alongside parameters such as porosity, water content, and thermal conductivity of the solid phase. Li et al. [7] proposed a multi-phase model for partially saturated cement-based porous composites, based on effective medium and mean-field theories, accounting for the pore shapes and orientations. Chu et al. [8] developed a fractal capillary bundle model at the pore scale for the effective thermal conductivity of porous geomaterials, considering structure parameters such as porosity,

* Corresponding author.
E-mail address: k.c.h.koh.chuen.hon@tue.nl (C.H. Koh).

https://doi.org/10.1016/j.ijheatmasstransfer.2024.126138
Received 12 June 2024; Received in revised form 6 August 2024; Accepted 28 August 2024

Nomenclatures

λ_{eff}	($W{\cdot}m^{-1}{\cdot}K^{-1}$) effective thermal conductivity
λ_1	($W{\cdot}m^{-1}{\cdot}K^{-1}$) thermal conductivity of the first phase
λ_2	($W{\cdot}m^{-1}{\cdot}K^{-1}$) thermal conductivity of the second phase
λ_s	($W{\cdot}m^{-1}{\cdot}K^{-1}$) thermal conductivity of the solid phase
λ_g	($W{\cdot}m^{-1}{\cdot}K^{-1}$) thermal conductivity of the gas phase
λ_w	($W{\cdot}m^{-1}{\cdot}K^{-1}$) thermal conductivity of the water phase
λ_a	($W{\cdot}m^{-1}{\cdot}K^{-1}$) thermal conductivity of air
λ_{dry}	($W{\cdot}m^{-1}{\cdot}K^{-1}$) effective dry thermal conductivity
λ_{sat}	($W{\cdot}m^{-1}{\cdot}K^{-1}$) effective saturated thermal conductivity
x_2	(-) contribution fraction of the second phase
x_g	(-) contribution fraction of the gas phase
x_w	(-) contribution fraction of the water phase
φ	(-) porosity
S_r	(-) degree of saturation
w	(-) water content
ρ	($kg{\cdot}m^{-3}$) bulk density
ρ_r	($kg{\cdot}m^{-3}$) relative density with respect to water

tortuosity, pore size distribution and its fractal dimension. For moist silica aerogel, Chen et al. [9] proposed a fractal-intersection sphere with an inhomogeneous water film structural model. Theoretical frameworks are also available on other porous mediums, such as soils and rocks. Ghanbarian and Daigle [10] proposed a model to predict thermal conductivity in these moist porous media based on percolation theory and effective medium theory.

While these generalized models provide analytical solutions for approximating the thermal conductivity of moist material, they often involve parameters that are challenging to obtain, such as the thermal conductivity for the solid phase and pore size distribution. Therefore, a generalized model based on commonly measured parameters would be more practical for implementation.

This study aims to derive a generalized moisture-dependent thermal conductivity solution for porous insulation material, using only commonly measured and readily available parameters. Existing multiphase models for porous materials, as reviews by Carson et al. [11] and Smith et al. [12] are referenced when deriving solutions for moist porous materials. The derived solutions are further validated with experimental data from the literature.

2. Model development

2.1. Two-phase models for effective thermal conductivity

The effective thermal conductivity (λ_{eff}) of air and water-filled porous materials can be approximated using a multiphase model approach. In a simplistic depiction, a dry porous material consists of a solid phase and a gas phase, while a fully saturated porous material comprises a solid phase and a water phase. This reduces the multiphase model to a two-phase model. Numerous analytical solutions exist for this model, each hinging on different assumptions regarding geometry and heat conduction pathways. Typically, these models involve three primary parameters: the thermal conductivity of the first phase (λ_1), typically assigned to the solid phase (λ_s); the thermal conductivity of the second phase (λ_2), typically assigned to the fluid phase in the pores,

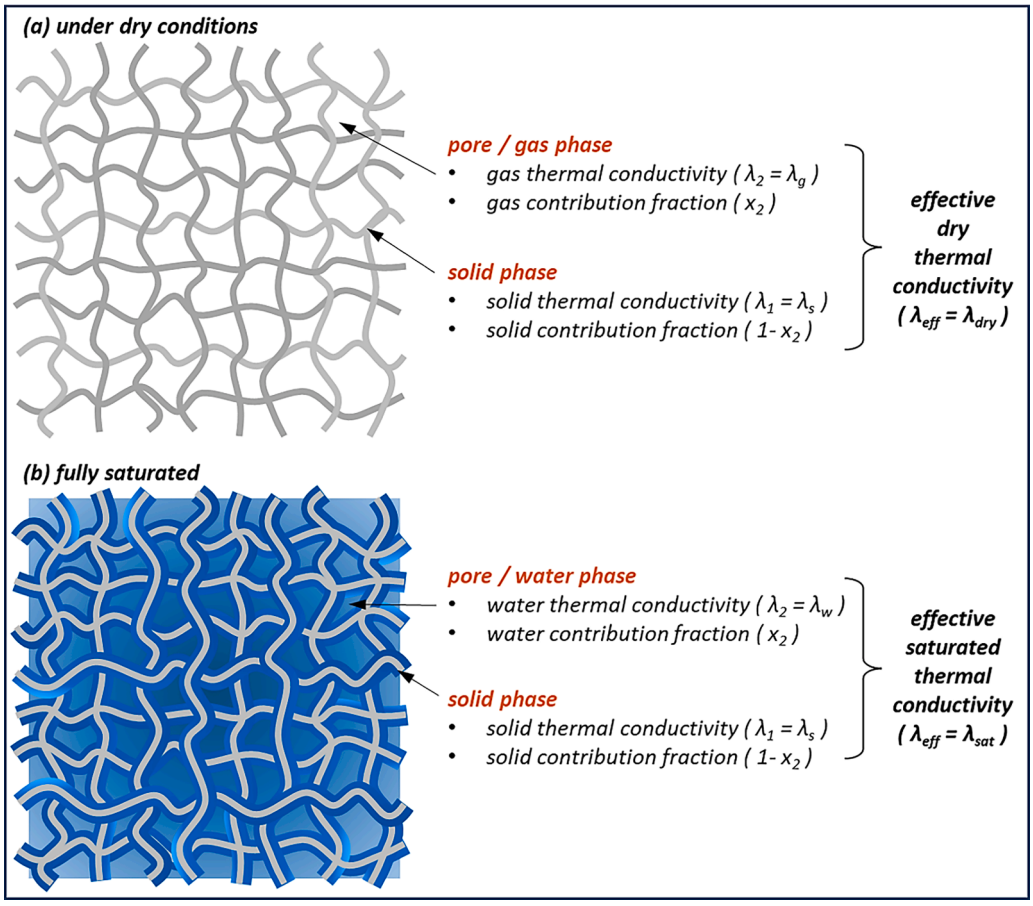

Fig. 1. Porous materials under both dry and fully saturated conditions, with the primary components when using a multiphase model approach. The depicted two-dimensional structure of the porous material is purely illustrative, and the actual structure could be fibrous, foam-like, or any other form of porous structure.

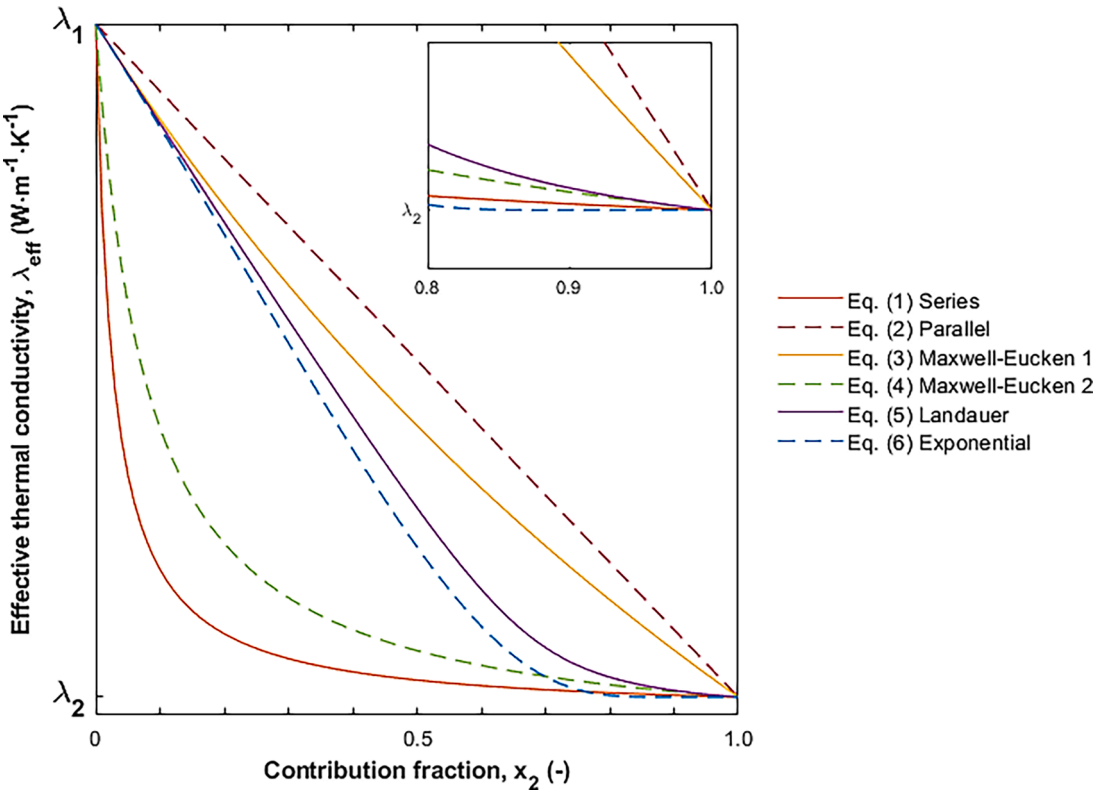

Fig. 2. Different two-phase model approaches for effective thermal conductivity.

Table 1
Parameters of four highly porous insulation materials [21] for the calculation.

	Stone wool	Glass fibres	PU foam	Expanded cork
Measured values from [21]				
Dry thermal conductivity, λ_{dry} ($W{\cdot}m^{-1}{\cdot}K^{-1}$)	0.040	0.035	0.030	0.040
Saturated thermal conductivity, λ_{sat} ($W{\cdot}m^{-1}{\cdot}K^{-1}$)	0.60	0.61	0.60	0.60
Porosity, φ (-)	0.95	0.99	0.95	0.9
Density, ρ ($kg{\cdot}m^{-3}$)	60	30	40	150
Estimated values				
Solid Thermal conductivity, λ_s ($W{\cdot}m^{-1}{\cdot}K^{-1}$)	3 [22]	1.4 [23]	0.21 [24]	0.4 [25]
Water Thermal conductivity, λ_w ($W{\cdot}m^{-1}{\cdot}K^{-1}$)	0.6 [20]			
Air Thermal conductivity, λ_a ($W{\cdot}m^{-1}{\cdot}K^{-1}$)	0.026 [20]			

Table 2
Calculated contribution fraction (x_2) using Eqs. (1) to (2) based on λ_{dry}, λ_s and λ_a from Table 1.

	Calculated x_2		Measured Porosity φ
Equations	Series, Eq. (1)	Parallel, Eq. (2)	
Stone wool	0.6469	0.9953	0.95
Glass fibres	0.7380	0.9934	0.99
PU foam	0.8478	0.9783	0.95
Expanded cork	0.6257	0.9626	0.90

either gas (λ_g) or water (λ_w); and the contribution fraction of the second phase (x_2). Generally, x_2 is assumed to be equivalent to the physical volume fraction of the pore, also known as porosity (φ) [11,12]. Fig. 1 illustrates a porous material under both dry and fully saturated

Table 3
Calculated saturated thermal conductivity (λ_{sat}) using Eqs. (1) and (2) based on x_2 (Table 2) and φ (Table 1).

	Calculated λ_{sat}				Measured λ_{sat}
Equations	Series, Eq. (1)	Parallel, Eq. (2)	Series, Eq. (1)	Parallel, Eq. (2)	
	$x_{2,eq1}$	$x_{2,eq2}$	φ	φ	–
Stone wool	0.8362	0.6113	0.6250	0.7200	0.60
Glass fibres	0.7056	0.6052	0.6034	0.6080	0.61
PU foam	0.4678	0.5915	0.5490	0.5805	0.60
Expanded cork	0.5054	0.5925	0.5714	0.5800	0.60

Table 4
Parameters of four medium-density materials [21] for the calculation.

	Peat [26]	Sand [26]	Concrete [27]	Clay-cement [28]
Measured values from				
Dry thermal conductivity, λ_{dry} ($W{\cdot}m^{-1}{\cdot}K^{-1}$)	0.10	0.15	0.42	0.43
Saturated thermal conductivity, λ_{sat} ($W{\cdot}m^{-1}{\cdot}K^{-1}$)	0.73	1.85	1.16	1.50
Porosity, φ (-)	0.77	0.55	0.20	0.48
Density, ρ ($kg{\cdot}m^{-3}$)	600	1200	2142	1283
Estimated values				
Solid Thermal conductivity, λ_s ($W{\cdot}m^{-1}{\cdot}K^{-1}$)	1.06	7.5	1.65	3.2
Water Thermal conductivity, λ_w ($W{\cdot}m^{-1}{\cdot}K^{-1}$)	0.6 [20]			
Air Thermal conductivity, λ_a ($W{\cdot}m^{-1}{\cdot}K^{-1}$)	0.026 [20]			

Table 5
Calculated contribution fraction (x_2) using Eqs. (1), (2) and (5) based on λ_{dry}, λ_s and λ_a from Table 4.

Equations	Calculated x_2			Measured Porosity φ
	Series, Eq. (1)	Parallel, Eq. (2)	Landauer, Eq. (5)	
Peat	0.2414	0.9284	0.6994	0.77
Sand	0.1676	0.9841	0.7113	0.55
Concrete	0.0469	0.7574	0.5206	0.20
Clay-cement	0.0528	0.8727	0.5994	0.48

conditions, along with the primary components when applying a multiphase model to predict λ_{eff}.

Six models derived from multiphase models, as reviewed by Carson et al. [11] and Smith et al. [12], are included in this study, illustrated in Fig. 2.

Among the various two-phase models, the simplest approach to predict λ_{eff} involves treating the solid and fluid as thermal resistors either in series or in parallel with respect to the heat flow, as expressed in:

$$\lambda_{eff} = \frac{1}{(1-x_2)/\lambda_1 + x_2/\lambda_2} \tag{1}$$

and

$$\lambda_{eff} = \lambda_1(1-x_2) + \lambda_2 x_2 \tag{2}$$

respectively. Although these assumptions neglect physical interaction between phases, they provide lower and upper bounds for effective thermal conductivity (Fig. 2).

Another well-established model is the Maxwell-Eucken relation [13], equivalent to the Hanshin-Shtrikman upper and lower bounds [14], and can be represented by:

$$\lambda_{eff} = \lambda_1 \frac{\lambda_2 + 2\lambda_1 - 2(\lambda_1 - \lambda_2)x_2}{\lambda_2 + 2\lambda_1 + (\lambda_1 - \lambda_2)x_2} \tag{3}$$

and

Table 6
Calculated saturated thermal conductivity (λ_{sat}) using Eqs. (1), (2) and (5) based on x_2 (Table 5) and φ (Table 4).

Equations	Calculated λ_{sat}						Measured λ_{sat}
	Series, Eq. (1) $x_{2,eq1}$	Parallel, Eq. (2) $x_{2,eq2}$	Landauer, Eq. (5) $x_{2,eq5}$	Series, Eq. (1) φ	Parallel, Eq. (2) φ	Landauer, Eq. (5) φ	–
Peat	0.8945	0.6329	0.7194	0.6654	0.7041	0.6886	0.73
Sand	2.5619	0.7168	1.4214	1.0287	3.7257	2.4550	1.85
Concrete	1.5249	0.8547	1.0169	1.2222	1.4400	1.3909	1.16
Clay-cement	2.6045	0.9309	1.3005	1.0390	1.9520	1.6204	1.50

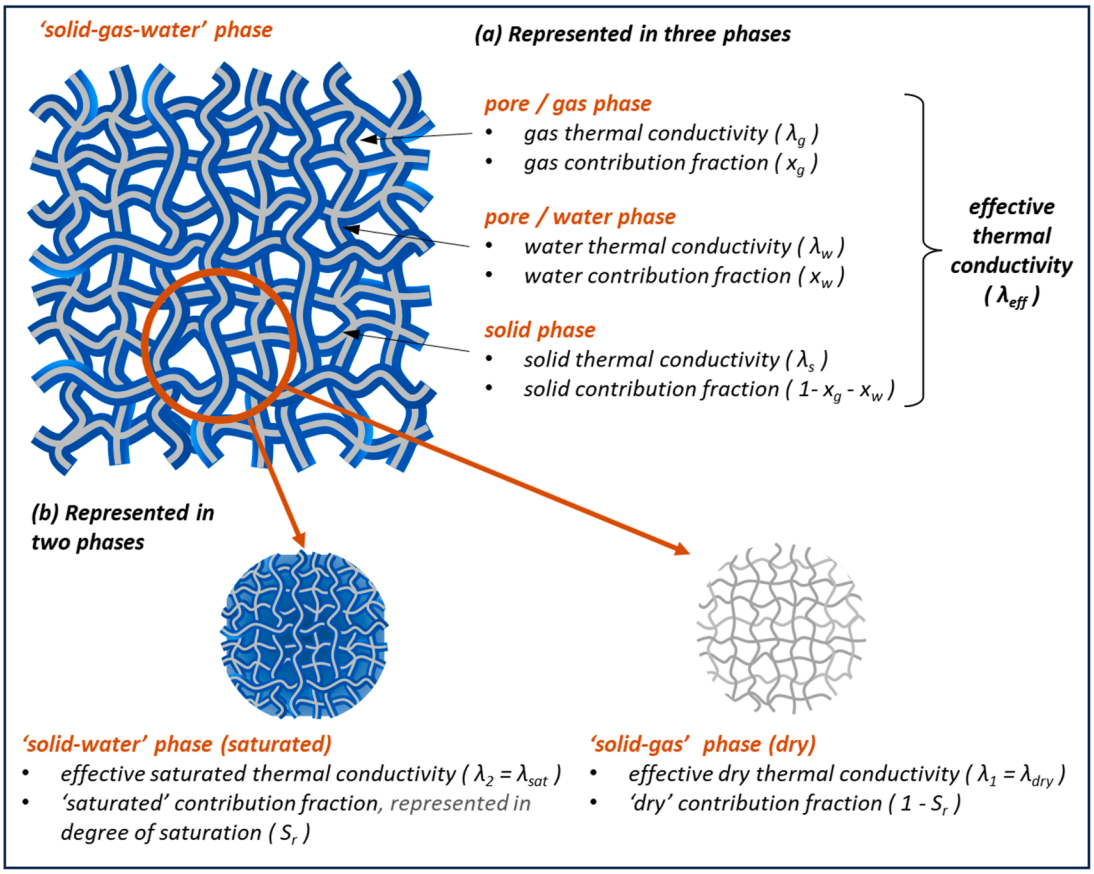

Fig. 3. Effective thermal conductivity for moist materials represented in (a) three phases, and (b) two phases.

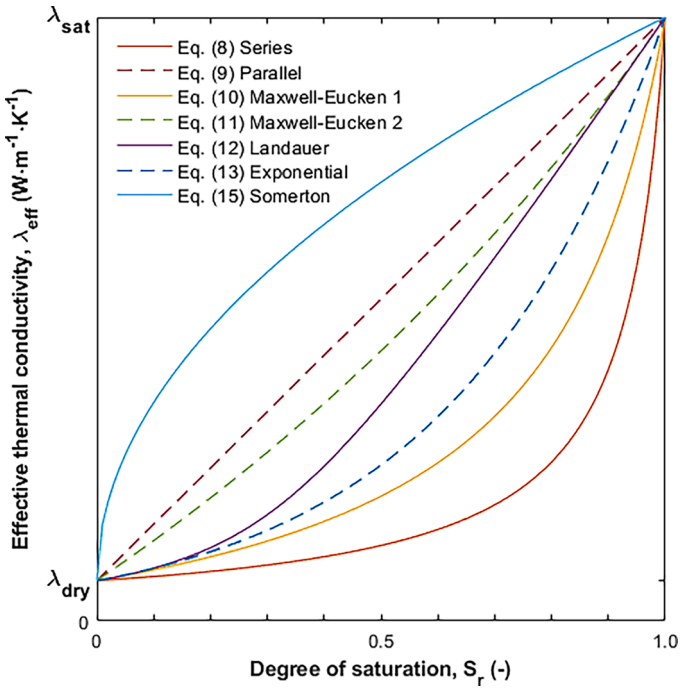

Fig. 4. Different two-phase model approaches for effective thermal conductivity under moist conditions.

$$\lambda_{eff} = \lambda_2 \frac{\lambda_1 + 2\lambda_2 - 2(\lambda_2 - \lambda_1)(1 - x_2)}{\lambda_1 + 2\lambda_2 + (\lambda_2 - \lambda_1)(1 - x_2)} \tag{4}$$

respectively. This model delineates upper and lower limits for the effective thermal conductivity of macroscopically homogeneous and isotropic multiphase materials, in terms of phase volume fraction and phase conductions. The model assumes individual closed pores dispersed uniformly in the solid matrix and does not account for a continuous conduction pathway through pores. The Maxwell-Eucken bounds further refine the estimated range, falling within the bounds set by Eqs. (1) and (2), as shown in Fig. 2.

Another approach, proposed by Landauer [15], is based on a random mixture assumption, treating each phase as if surrounded by a homogeneous medium with properties are the mixture. The model allows open porosity where the interconnected pore phase forms a continuous heat conduction pathway, leading to a stronger dependence of thermal conductivity on the pore phase. This solution, known also as the Effective Medium Theory (EMT), can be expressed either in its implicit form as follows:

$$(1 - x_2)\frac{\lambda_1 - \lambda_{eff}}{\lambda_1 + 2\lambda_{eff}} + x_2\frac{\lambda_2 - \lambda_{eff}}{\lambda_2 + 2\lambda_{eff}} = 0 \tag{5}$$

alternatively, in its explicit form as follows:

$$\lambda_{eff} = \frac{1}{4}\left\{\lambda_2(3x_2 - 1) + \lambda_1(2 - 3x_2) + \sqrt{[\lambda_2(3x_2 - 1) + \lambda_2(2 - 3x_2)]^2 + 8\lambda_1\lambda_2}\right\} \tag{5a}$$

The solution sits within the bounds set by Eqs. (3) and (4), however, do not universally fit all measurements examined in the original study.

A simple exponential relation, proposed by Tichá et al. [16], assumes a closed-pores microstructure with non-conducting pores, therefore eliminating the parameter λ_2. However, the proposed equation breaks down at a higher pore volume fraction and approaches zero. This breakdown can be mitigated by reconsidering the effect of the thermal conductivity of the second phase and is expressed by:

$$\lambda_{eff} = (\lambda_1 - \lambda_2)\cdot exp\left(\frac{-Bx_2}{1 - x_2}\right) + \lambda_2 \tag{6}$$

where the parameter B relates to pore shape, with $B = 3/2$ assumed for spherical pores.

λ_s for inorganic minerals vary widely depending on mineral composition and crystal orientation, ranging from 1 to 5 $W{\cdot}m^{-1}{\cdot}K^{-1}$ [17], and up to 10 $W{\cdot}m^{-1}{\cdot}K^{-1}$ for quartz with crystal orientation parallel to the heat source [18]. Organic solid matter has lower λ_s values, ranging from 0.13 to 0.35 $W{\cdot}m^{-1}{\cdot}K^{-1}$ [19]. For insulation materials filled with air, λ_g is typically equivalent to the thermal conductivity of air (λ_a), around 0.026 $W{\cdot}m^{-1}{\cdot}K^{-1}$ at 20 °C [20]. For a fully saturated porous material, λ_w is approximately 0.6 $W{\cdot}m^{-1}{\cdot}K^{-1}$ at 20 °C [20].

2.2. *Effective saturated thermal conductivity*

2.2.1. *Highly porous insulation materials*

For building insulation materials, the effective saturated thermal conductivity (λ_{sat}) is less commonly measured and investigated compared to the effective dry thermal conductivity (λ_{dry}), both commercially and in the literature. Theoretically, a fully saturated porous material can be simplified as a two-phase model by assuming all pores are filled with water in their saturated state. The same equations (Eqs. (1) to (6)) should provide a valid prediction for λ_{sat} based on the same contribution fraction x_2 used to predict λ_{dry}. To validate this assumption, Eqs. (1) and (2), representing the lower and upper bounds for λ_{dry} (Fig. 2), are used to calculate λ_{sat} and compared against their measured λ_{sat}. Four highly porous insulation materials from the open-source MASEA database [21] are selected, and the parameters of these materials used in the calculations are listed in Table 1.

When applying Eqs. (1) to (6) to predict λ_{dry}, x_2 is generally assumed to be equivalent to the physical porosity (φ). Table 2 presents the calculated x_2 for the pore when applying Eqs. (1) and (2) based on measured λ_{dry}, and λ_s and λ_a obtained from the literature. The calculated x_2 from Eqs. (1) and (2) form the lower and upper limits for the measured φ, and it appears that the prediction of x_2 following Eq. (2) is closer to φ.

λ_{sat} is further predicted based on x_2 calculated from Table 2 and compared to λ_{sat} calculated from the measured φ. Here, the second phase is the water phase. Both sets are then compared against the measured λ_{sat}. The results are listed in Table 3. Among all four calculations, λ_{sat} calculated from x_2 using Eq. (2) is closer to the measured λ_{sat}, aligning with the lower boundary close to the second phase (λ_w at 0.6 $W{\cdot}m^{-1}{\cdot}K^{-1}$). In contrast, λ_{sat} calculated from the measured φ significantly deviates from the measured λ_{sat}. This deviation suggests the limitation of using porosity (φ) as x_2 in estimating λ_{eff}. It should also be noted that the physical pore volume accessible to water is not always the same as the total pore volume that can be filled by gas (air).

Despite the varying λ_s value (0.21 to 3 $W{\cdot}m^{-1}{\cdot}K^{-1}$), all samples exhibit a similar range in λ_{sat}. This similarity indicates that the influence of the solid phase's thermal conductivity has little effect on the thermal conductivity of saturated insulation material, aligning with findings from [6]. This is evident from the MASEA database [21], where the majority of porous materials have λ_{sat} values close to λ_w.

Based on these findings, in the absence of direct λ_{sat} measurement, λ_{sat} can be approximated using the parallel relation. The contribution fraction x_2 is first estimated using Eq. (2) with λ_{dry}, λ_s, and λ_a as inputs. Then, λ_{sat} is approximated using the same Eq. (2) with the calculated x_2, λ_s and λ_w as the inputs. It appears that λ_{sat} is often close to the boundary of the second phase (λ_w). Therefore, when λ_s is not known, it is reasonable to equate λ_{sat} to λ_w for highly porous materials.

2.2.2. *Medium-density materials*

The λ_{sat} approximation is further applied to four medium-density materials [26,27,28], typical examples are clay and sand, and

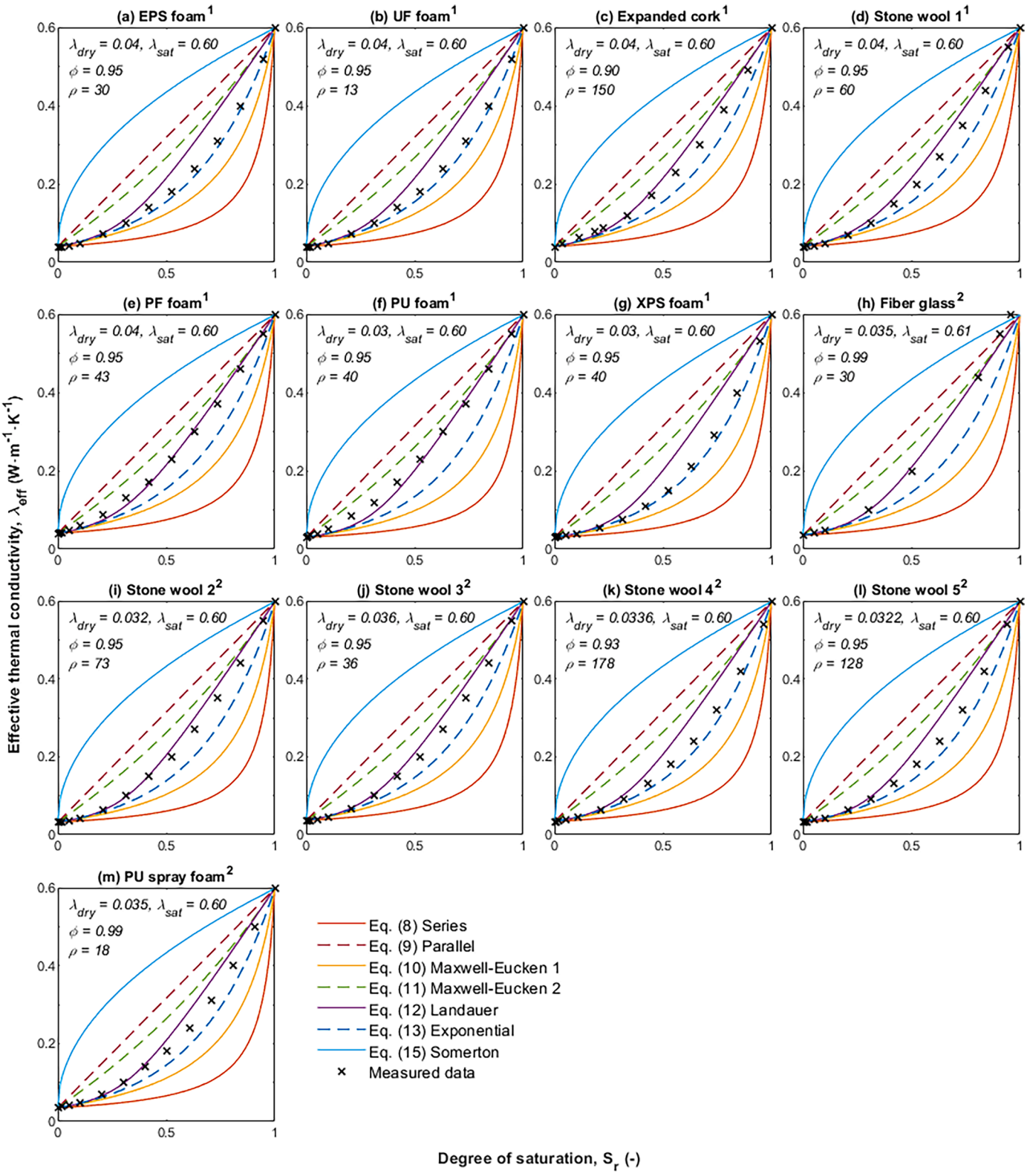

Fig. 5. Analytical solutions to approximate moisture-dependent thermal conductivities using Eqs. (8) to (15), in comparison to measurement data of different porous insulation materials from the MASEA database from Fraunhofer-IBP (denoted 1) and material database from WUFI (denoted 2).

cement-based construction materials such as mortar and concrete. The parameters of these materials used in the calculations are listed in Table 4.

The prediction of x_2 from Eqs. (1) and (2) significantly deviate from the measured φ (Table 5). However, it is observed that the measured φ falls between the calculated x_2 values from Eqs. (1) and (2). To provide a more accurate approximation, Landauer's relation (Eq. (5)), also known as Effective Medium Theory, is included as well. The prediction of x_2 following Eq. (5) is shown to be closer to φ.

The calculated λ_{sat} based on the calculated x_2 (Table 5) and the

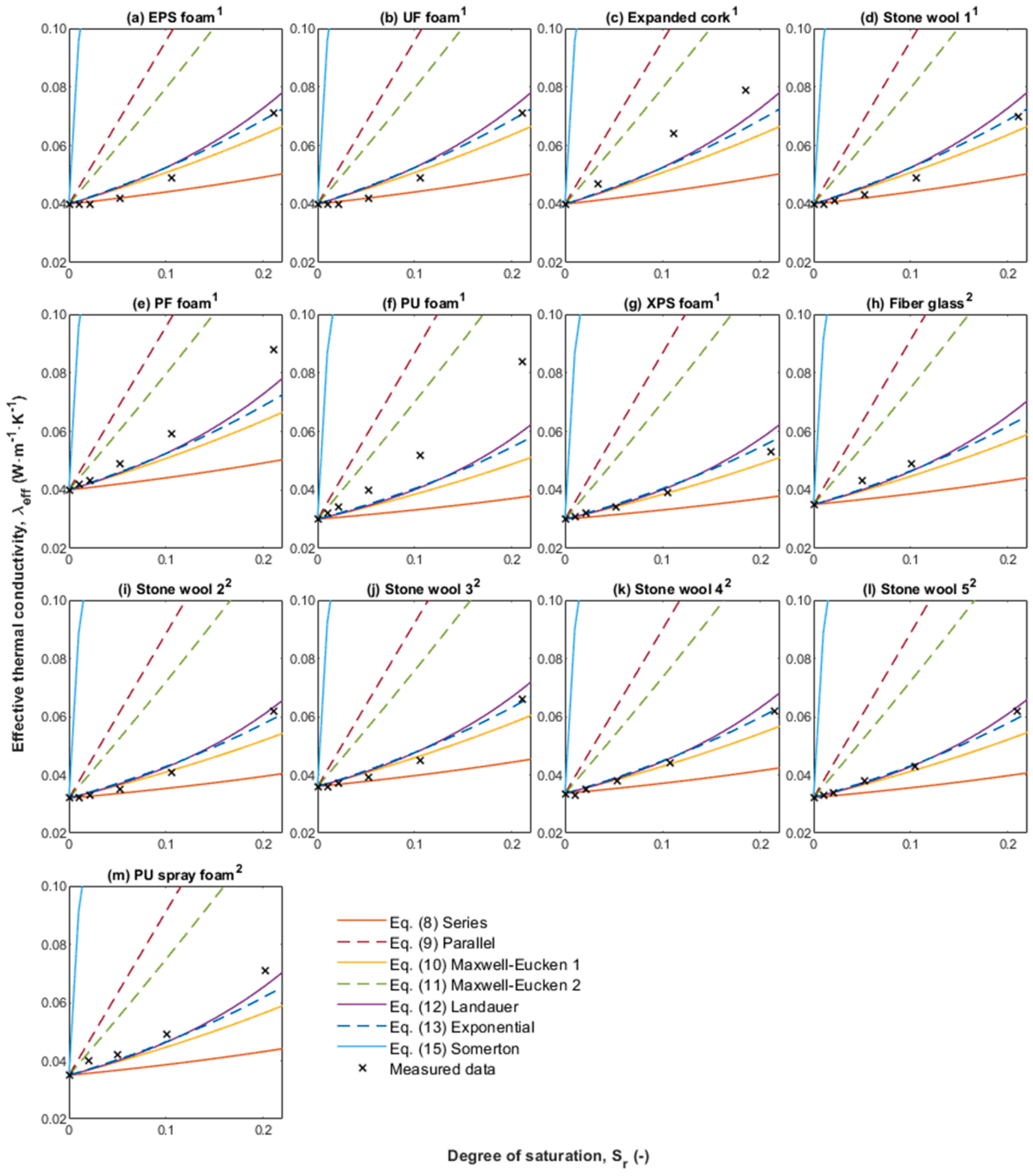

Fig. 6. Similar to Fig. 5, but focusing only on lower degrees of saturation.

measure φ are listed in Table 6. Similarly, λ_{sat} calculated from x_2 using Eq. (5) is closer to the measured λ_{sat}. Additionally, Eq. (5) forms the lower bound for the λ_{sat} estimation, while Eq. (1) remains the upper bound.

Based on these findings, in the absence of direct λ_{sat} measurement, λ_{sat} can be approximated using Landauer's relation for medium-density materials. However, its accuracy is lower than applying the parallel relation on highly porous materials.

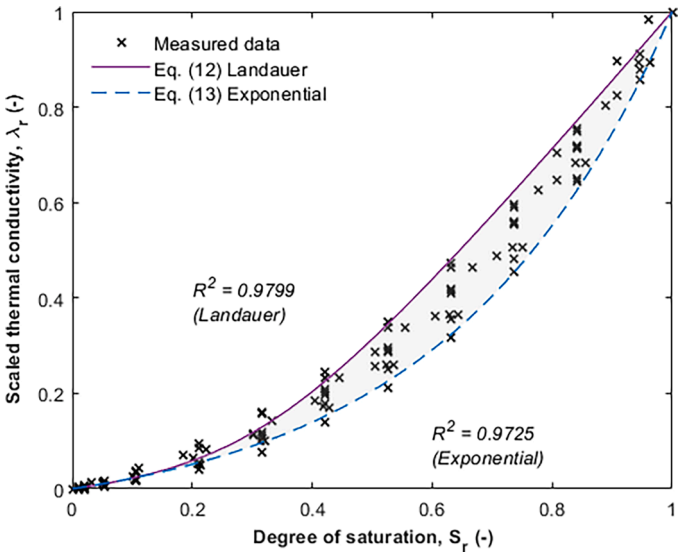

Fig. 7. Scaled thermal conductivity (Eq. (17)) versus degree of saturation (S_r) for Eqs. (12) and (13), plotted against the overall measured data from Fig. 5 with the corresponding coefficient of determination R^2.

two-phase model characterized by two parameters: effective dry thermal conductivity (λ_{dry}, where $S_r = 0$) and effective saturated thermal conductivity (λ_{sat}, where $S_r = 1$). λ_{dry} and λ_{sat} form the lower and upper boundary limits, respectively, of $\lambda_{eff}(S_r)$. This approach eliminates the need for the solid phase parameter (λ_s). Measuring λ_s for a continuous solid state without any pore spaces in a porous material is impractical [29]. Moreover, λ_s values based on the main constituents of a material provide only an approximation.

Based on these assumptions, the two-phase models are adapted for effective thermal conductivity, $\lambda_{eff}(S_r)$, as follows:

$$\lambda_{eff}(S_r) = \frac{1}{(1-S_r)/\lambda_{dry} + S_r/\lambda_{sat}} \tag{8}$$

$$\lambda_{eff}(S_r) = \lambda_{dry}(1-S_r) + \lambda_{sat}S_r \tag{9}$$

$$\lambda_{eff}(S_r) = \lambda_{dry}\frac{\lambda_{sat} + 2\lambda_{dry} - 2(\lambda_{dry} - \lambda_{sat})S_r}{\lambda_{sat} + 2\lambda_{dry} + (\lambda_{dry} - \lambda_{sat})S_r} \tag{10}$$

$$\lambda_{eff}(S_r) = \lambda_{sat}\frac{\lambda_{dry} + 2\lambda_{sat} - 2(\lambda_{sat} - \lambda_{dry})(1-S_r)}{\lambda_{dry} + 2\lambda_{sat} + (\lambda_{sat} - \lambda_{dry})(1-S_r)} \tag{11}$$

and

$$\lambda_{eff}(S_r) = \frac{1}{4}\left\{\lambda_{sat}(3S_r - 1) + \lambda_{dry}(2 - 3S_r) + \sqrt{\left[\lambda_{sat}(3S_r - 1) + \lambda_{dry}(2 - 3S_r)\right]^2 + 8\lambda_{dry}\lambda_{sat}}\right\} \tag{12}$$

2.3. Adaptation of multiphase solid-gas-water models to two-phase models

A partially saturated porous material consists of three distinct phases: solid, water and gas, as illustrated in Fig. 3a. Within the pores, both water vapour and condensed water are treated as a single water phase. Analytical solutions for these tri-phase systems can be derived from multiphase models. This study simplifies the tri-phase solutions into two-phase solutions by introducing two arbitrary phases: the 'solid-water' phase and the 'solid-gas' phase, corresponding to saturated and dry conditions, respectively, as shown in Fig. 3b.

The three-phase moist material is transformed into two separate two-phase components. The 'solid-water' phase is represented by the effective saturated thermal conductivity (λ_{sat}) and an arbitrary contribution fraction (x_2); the 'solid-gas' phase is represented by the effective dry thermal conductivity (λ_{dry}) and a corresponding arbitrary contribution fraction (1 - x_2). The arbitrary contribution fraction x_2 is assumed to be proportional to the physical degree of saturation (S_r) in the moist porous material. By assuming a similar volume fraction of the solid phase is allocated to the 'solid-water' phase, x_2 is equivalent to S_r. Similarly, the contribution fraction for the 'solid-gas' phase can be equated to $(1 - S_r)$. The relationship between S_r and water content (w in kg water / kg dry material) can be described using:

$$S_r = \frac{w \cdot \rho_r}{\phi} \tag{7}$$

where ρ_r is the relative density of the dry porous material with respect to water (specific density of solid divided by water density), and φ is the amount of pore volume accessible to water. $\varphi = 1$ represents the maximum amount of water the material can absorb in its saturated state, where $S_r = 1$. φ is typically equivalent to open porosity but should include closed pores with vapour-permeable walls that are also accessible to water vapour.

This reduction transforms the tri-phase moist porous model into a

Additionally, the exponential function in Eq. (7) is modified to:

$$\lambda_{eff}(S_r) = \lambda_{dry} \cdot exp(B' S_r) \tag{13}$$

with B' defined as:

$$B' = ln\left(\frac{\lambda_{sat}}{\lambda_{dry}}\right) \tag{14}$$

An empirical relation based on Somerton et al. [30,31] is included for comparison, suggesting the following correlation:

$$\lambda_{eff}(S_r) = \lambda_{dry}\left(1 - \sqrt{S_r}\right) + \lambda_{sat}\sqrt{S_r} \tag{15}$$

This relation is derived from partially brine-saturated quartz sand. This model follows a similar parallel relation but assigns a higher contribution fraction to the saturation phase.

These models are illustrated in Fig. 4. Similar to the initial models, both series and parallel relations form the outermost lower and upper bounds, followed by the Maxwell-Eucken relations. Both Landauer's and exponential relations fall within the bounds of Maxwell-Eucken's relation. However, the Somerton relation is an outlier, suggesting a higher λ_{eff} than the parallel model.

The equations for $\lambda_{eff}(S_r)$ require only two parameters: λ_{dry} ($S_r = 0$) and λ_{sat} ($S_r = 1$). The λ_{dry} is a commonly measured property for insulation materials. As discussed in the previous section, for highly porous material, λ_{sat} can be approximated using parallel relation with λ_{dry}, λ_a and λ_s. The results, however, are close to λ_w. When λ_s is not known, it is therefore reasonable to equate λ_{sat} to λ_w for highly porous materials. By making this assumption, the estimation of $\lambda_{eff}(S_r)$ requires only one measured parameter, namely λ_{dry}.

Other critical environmental parameters, particularly temperature, are assumed to be independent and constant in this study. This assumption simplifies the model but could be revisited in future studies to account for the temperature dependence of thermal conductivity,

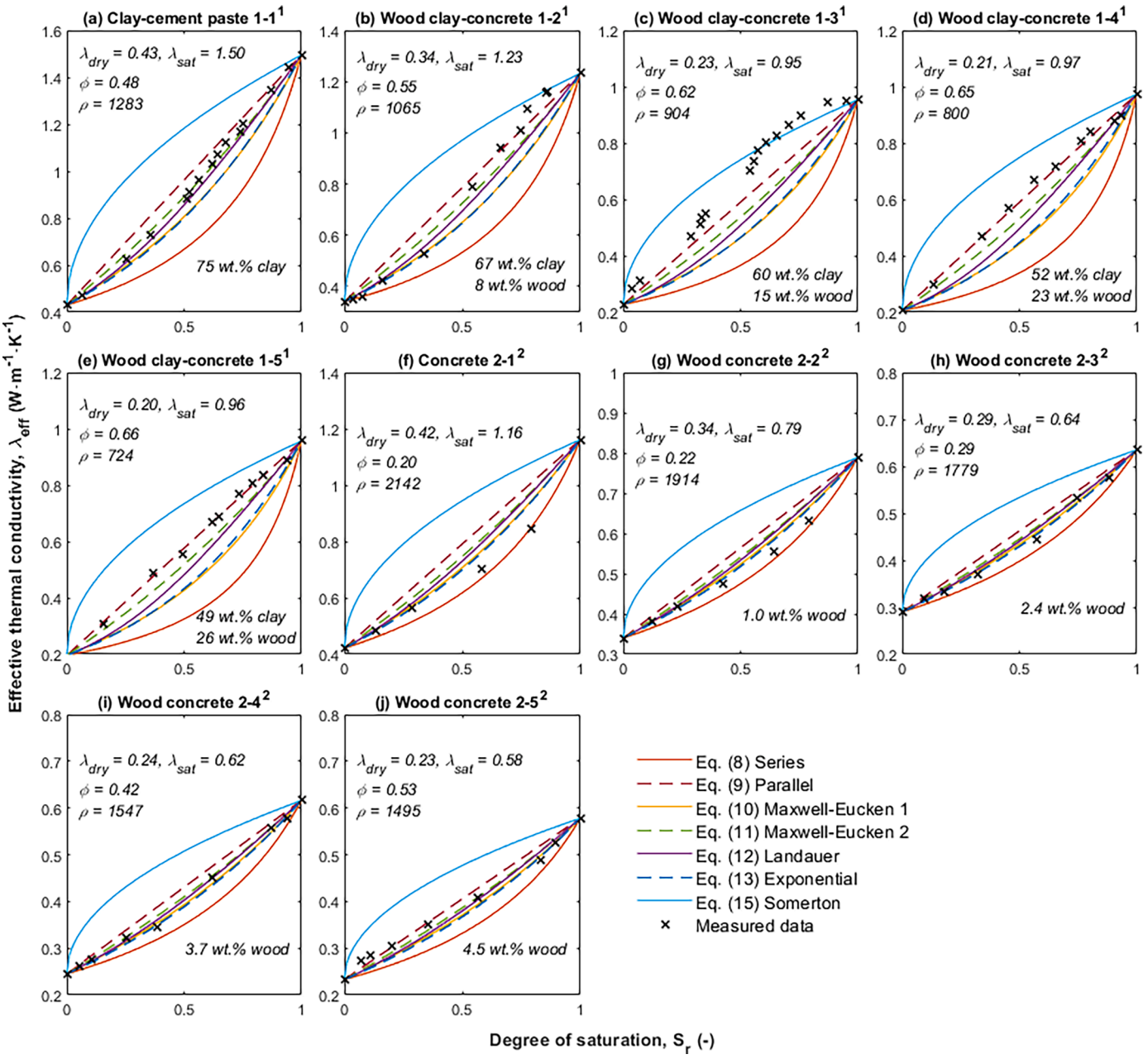

Fig. 8. Analytical solutions to approximate moisture-dependent thermal conductivities using Eqs. (8) to (15), in comparison to measurement data of different medium-density materials based on Bouguerra [28] (denoted 1) and Taoukil et al. [27] (denoted 2).

especially for materials and conditions where temperature variations are significant.

3. Results and discussion

3.1. Model validation to highly porous insulation materials

The validation of Eqs. (8) to (15) are conducted using materials featuring measured moisture-dependent thermal conductivity data. Two established sources are used for model validation: the open-source MASEA database [21] and a commercial database [32]. Only materials with measured moisture-dependent thermal conductivity are considered, leading to a selection of thirteen porous insulation materials. These materials include various types such as stone wools, expanded polystyrene (EPS) foam, urea-formaldehyde (UF) foam, expanded cork, phenolic (PF) foam, polyurethane (PU) foam, extruded polystyrene (XPS) foam and glass fibres. Materials with estimated properties are excluded from the analysis.

The measured moisture-dependent thermal conductivities are plotted against the corresponding degree of saturation (S_r), alongside the predicted values from Eqs. (8) to (15), as depicted in Fig. 5. The S_r is converted from water content (w) using Eq. (7) based on the measured porosity (φ) and bulk density (ρ).

Overall, the measurement data generally falls within the upper and lower bounds set by both the series-parallel relations and Maxwell-Eucken's relations. The fittings also indicate the validity of equating contribution fraction x_2 to S_r in estimating λ_{eff} when applying Eqs. (8) to (15).

At lower degrees of saturation (up to 0.2), the insulation materials tend to exhibit effective thermal conductivities closer to the lower

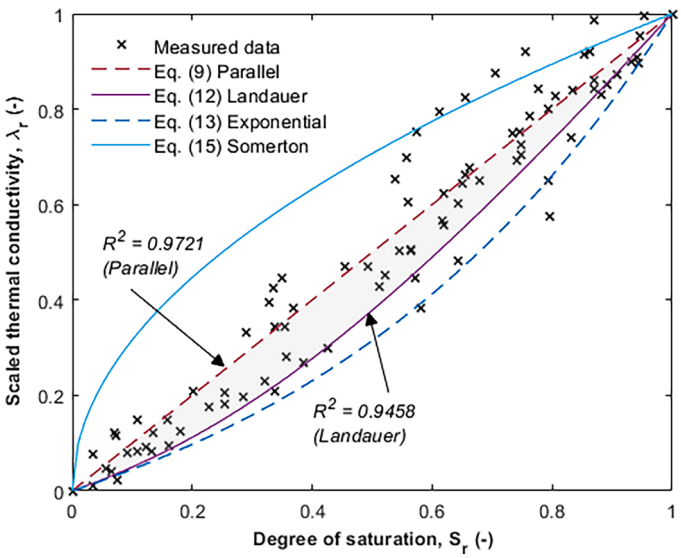

Fig. 9. Scaled thermal conductivity (Eq. (17)) versus degree of saturation (Sr) for Eqs. (9) and (12), plotted against the overall measured data from Fig. 8 with the corresponding coefficient of determination R2.

bounds. In some instances, they align with the series relation, as illustrated in Fig. 6. In this lower saturation range, the majority of the measurements follow the trends of Maxwell-Eucken-1's, exponential, and Landauer's relations.

As the moisture content increases further, the effective thermal conductivities demonstrate an exponential trend. Most of the data points fall within a narrower upper bound set by Landauer's relation and a lower bound set by exponential relations, as displayed in Fig. 5. It should be noted that the measurements do not follow the empirical square root correlation as suggested by Somerton. This could be due to the difference in porosity: Somerton's relation is derived based on material with porosity between 0.3 and 0.5, while the insulation materials investigated in this section are highly porous ($\varphi \geq 0.9$).

Upon overall assessment, the measurement data does not perfectly conform to the derived solutions based on Eqs. (8) to (15). Nevertheless, the trends are notably consistent with an exponential trend. Specifically, the effective thermal conductivity increases gradually at lower moisture content levels and then exponentially approaches the thermal conductivity for a standalone water phase. Therefore, a single linear approximation would either underestimate the effective thermal conductivity at a lower water content range (if approximated using the entire water content range, similar to a parallel relation) or at a higher range (if approximated using only the lower water content range).

The analysis of the proposed solutions reveals that both Landauer's and exponential relations, represented by Eqs. (12) and (13), provide the best fits for the measured data. The scaled thermal conductivity (λ_r) is defined as follows:

$$\lambda_r(S_r) = \frac{\lambda_{eff}(S_r) - \lambda_{dry}}{\lambda_{sat} - \lambda_{dry}} \tag{17}$$

where λ_{dry} is the thermal conductivity for $S_r = 0$, and λ_{sat} is the one for $S_r = 1$. This is plotted against the corresponding S_r in Fig. 7. Both Landauer's and exponential relations exhibit a high average coefficient of determination (R^2), with values of 0.9799 and 0.9725 respectively. This indicates a strong correlation between the predicted and observed values. Furthermore, Eq. (12) could serve as the upper bound, while Eq. (13) could serve as the lower bound for the moisture-dependent thermal conductivity.

3.2. Model validation to medium-density materials

Eqs. (8) to (15) are further validated on different medium-density materials. Fig. 8 presents the moisture-dependent thermal conductivity for various concretes, specifically five different wood-clay concrete samples based on Bouguerra [28], and five different wood concrete samples from Taoukil et al. [27]. Fig. 10 shows the moisture-dependent thermal conductivity for ten different peat, soil, and sand samples based on He et al. [26]. The corresponding scaled thermal conductivity for Fig. 8 and Fig. 10 are plotted in Fig. 9 and Fig. 11, respectively.

The effective thermal conductivity of medium-density materials in Fig. 8 no longer falls within the narrower bounds set by Landauer's and exponential relations. Overall, the data are contained within the wider bounds set by Somerton's and exponential relations, with most of them further falling within narrower bounds set by parallel and Landauer's relation. Instead of an exponential trend exhibited by highly porous materials, the effective thermal conductivity of medium-density moist materials follows a linear trend, corresponding to an average R^2 of 0.9721 for the parallel relation, as shown in Fig. 9.

In contrast, the effective thermal conductivity of moist sand and soil follows more closely a square root trend, as shown in Fig. 10. This aligns with the empirical square root correlation suggested by Somerton. Somerton's relation exhibits an average R^2 of 0.9566, while the parallel relation has a lower R^2 of 0.8989. Both Somerton's and parallel relations can serve as upper and lower bounds, respectively, for soil and sand-type materials, as shown in Fig. 11.

3.3. Parametric study and discussion

Eqs. (8) to (15) utilize only two main parameters, namely effective dry thermal conductivity (λ_{dry}) and effective saturated thermal conductivity (λ_{sat}), without considering porosity, pore shapes, pore size distribution, or material types. From Fig. 5 to Fig. 11, a distinct pattern emerges, which is summarized in Fig. 12. For materials with low λ_{dry} (up to 0.05 $W{\cdot}m^{-1}{\cdot}K^{-1}$) and low λ_{sat} (around 0.6 $W{\cdot}m^{-1}{\cdot}K^{-1}$), their effective thermal conductivities fall within the narrow and lower boundaries set by exponential and Landauer's relations. For materials with higher λ_{dry} and λ_{sat}, such as medium-density materials, the distribution of their effective thermal conductivity becomes broader. The upper bound shifts higher, limited by the parallel relation, and in the case of soil and sand, by Somerton's relation. Similarly, the lower bound shifts upward, aligning with Landauer's relation, and for soil and sand, with the parallel relation.

When materials are categorized based on their bulk density (ρ) and porosity (φ), a similar pattern can be observed, as shown in Fig. 13. For materials with lower bulk densities (below 200 $kg{\cdot}m^{-3}$) and higher porosity (above 0.9), their thermal conductivities fall within the exponential and Landauer's relations. Additionally, materials with higher bulk densities and lower porosities exhibit effective thermal conductivities that generally follow a linear trend, albeit within a broader range.

For highly porous materials, the effective thermal conductivities do not show significant variation based on their constituents (organic or inorganic) or form (foam or fibrous mat). The low fraction of the solid phase in these materials diminishes the influence of the solid phase's thermal conductivity on their overall thermal conductivity. Due to their highly porous structure, the water phase does not form a continuous conduction path at a lower degree of saturation and only increases exponentially at a higher degree of saturation.

Conversely, the thermal conductivity of the solid phase plays a more significant role in the effective thermal conductivity of medium-density materials. It can be observed that sand and soils with higher silica (sand) content align more closely with the upper Somerton's relation, compared to samples with lower silica content, which are closer to a lower parallel relation (Fig. 10). The granulated form of these materials also contributes significantly. The presence of an additional water layer

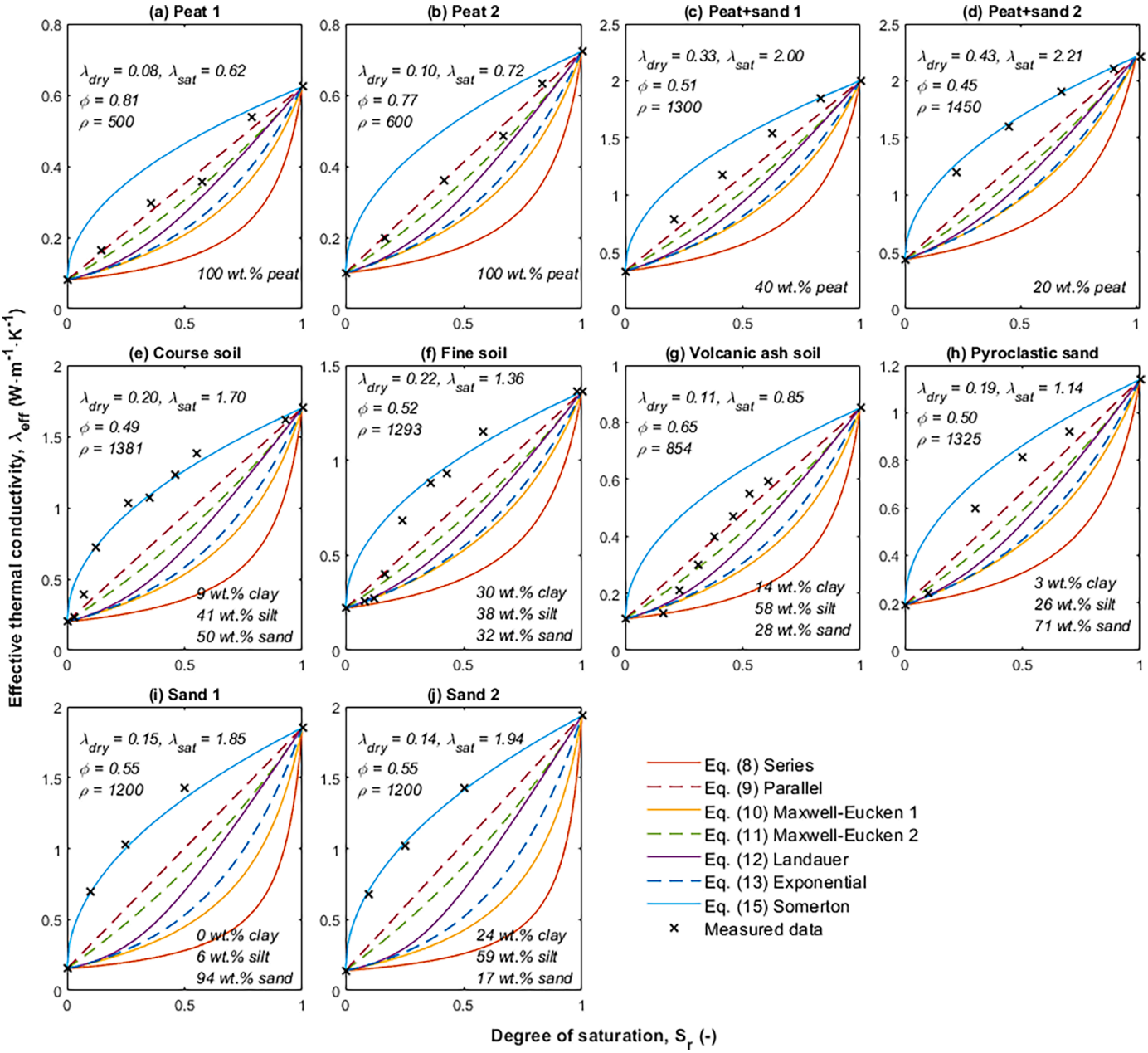

Fig. 10. Analytical solutions to approximate moisture-dependent thermal conductivities using Eqs. (8) to (15), in comparison to measurement data of different medium-density materials based on He et al. [26].

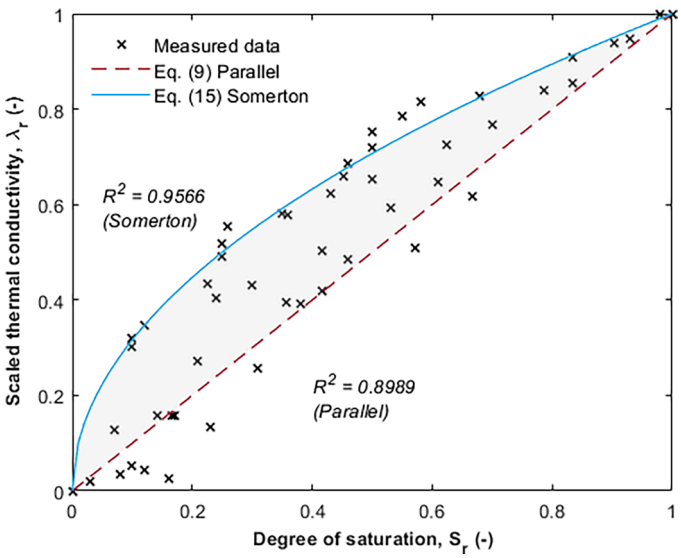

Fig. 11. Scaled thermal conductivity (Eq. (17)) versus degree of saturation (Sr) for Eqs. (9) and (15), plotted against the overall measured data from Fig. 10 with the corresponding coefficient of determination R2.

on granulated materials increases the surface area in contact with neighbouring particles, even at lower degrees of saturation, thereby enhancing the heat conduction paths, as indicated by Somerton's relation.

The broader range of effective thermal conductivity exhibited by the selected medium-density materials can be attributed to the inhomogeneous nature of the material constituents and microstructure, as well as moisture distribution in the moist materials. Additionally, the challenging measurement techniques used can introduce uncertainties to the results. This variability underscores the complexity of accurately predicting thermal conductivity in medium-density materials, highlighting the importance of considering both material composition and microstructural characteristics in thermal conductivity models.

4. Conclusion

A straightforward and robust two-phase method is proposed to predict moisture-dependent thermal conductivity (λ_{eff}) for porous materials, of medium and high porosity. This approach adapts six analytical solutions from the multiphase model, including series-parallel, Maxwell-Eucken, Landauer's, and exponential relations, for application to moist porous materials. By introducing an arbitrary effective dry phase and a saturated phase, the original tri-phase model, which includes solid, air, and water phases, is simplified into a two-phase model. This reduction streamlines the analysis and facilitates practical implementation.

The proposed method requires only two parameters to predict λ_{eff} under different degrees of saturation (S_r): effective dry thermal conductivity (λ_{dry}, where $S_r = 0$) and effective saturated thermal conductivity (λ_{sat}, where $S_r = 1$). λ_{dry} and λ_{sat} form the lower and upper boundary limits, respectively, of $\lambda_{eff}(S_r)$.

For highly porous materials ($\varphi \geq 0.9$), in the absence of direct λ_{sat} measurement, λ_{sat} can be obtained using the parallel relation. The contribution fraction x_2 is first estimated using Eq. (2) with λ_{dry}, λ_s, and λ_a as inputs. Then, λ_{sat} is approximated using the same Eq. (2) with the calculated x_2, λ_s and λ_w. It appears that λ_{sat} is often close to λ_w. Therefore, when λ_s is not known, it is reasonable to equate λ_{sat} to λ_w for highly porous materials. For medium-density materials, λ_{sat} can be obtained using Landauer's relation following the same procedure, though with a lower accuracy.

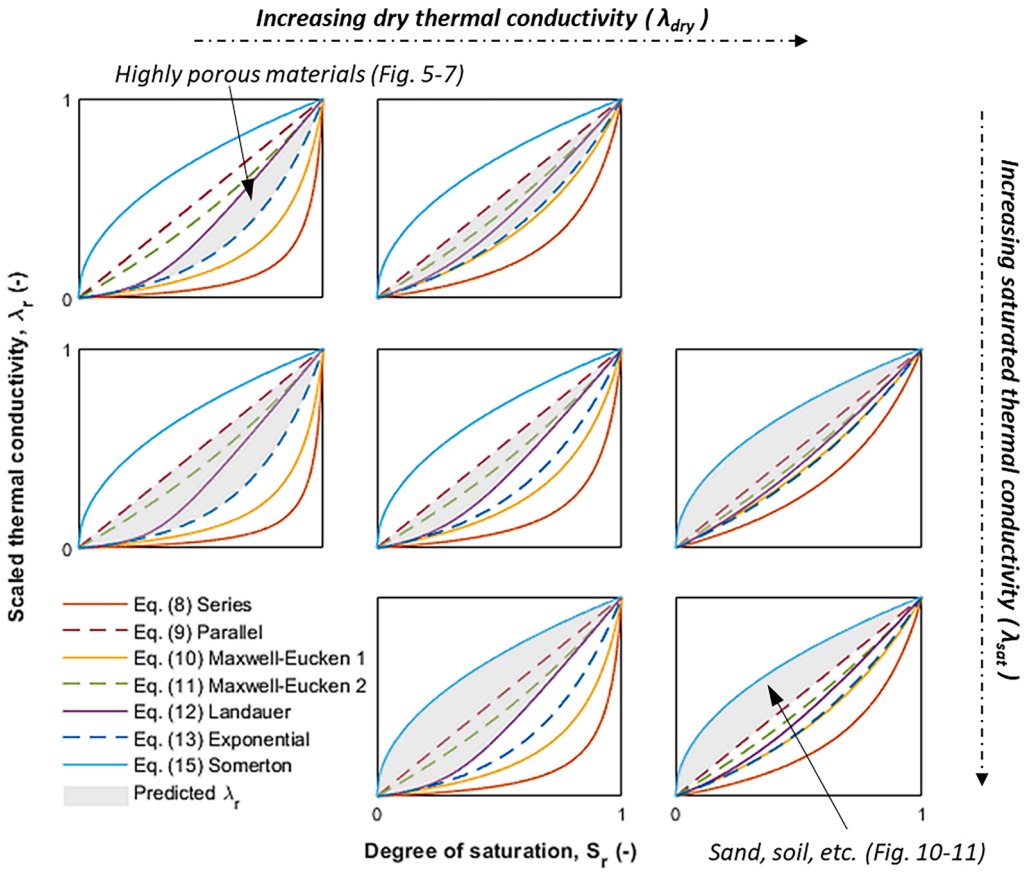

Fig. 12. Variations of scaled thermal conductivity with degrees of saturation at different dry thermal conductivity (λ_{dry}) and saturated thermal conductivity (λ_{sat}).

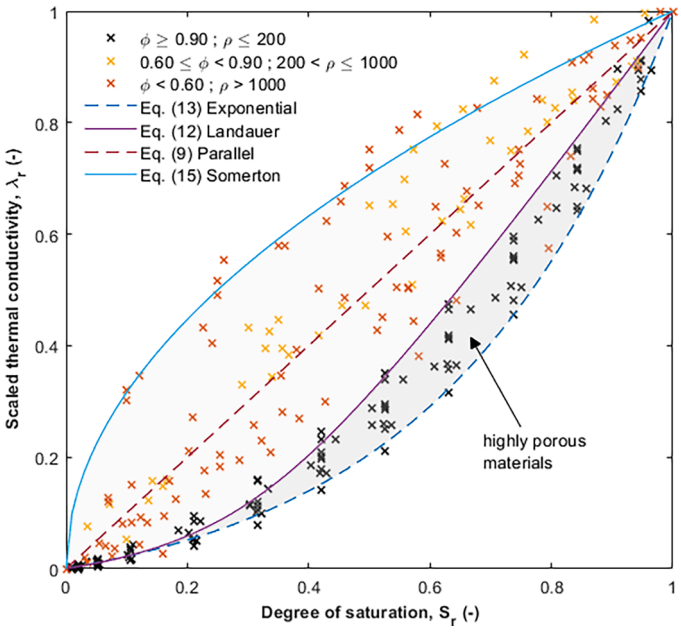

Fig. 13. Scaled thermal conductivity (Eq. (17)) versus degree of saturation (Sr) plotted against the overall measured data from Fig. 5, Fig. 8 and Fig. 10. The measured data are categorized based on their porosity (-) and density (kg·m^{-3}).

The validation results indicate that both Landauer's relation, Eq. (12), and exponential relation, Eq. (13), provide the best fit to the measured data of partially saturated highly porous media, with average coefficients of determination (R^2) at 0.9799 and 0.9725, respectively. Moreover, Landauer's relation can serve as the upper bound, while the exponential relation can serve as the lower bound for moisture-dependent thermal conductivity.

For medium-density materials, the distribution of their effective thermal conductivity becomes broader. The upper bound aligns with the parallel relation and, in the case of soil and sand, with Somerton's relation. The lower bound aligns with Landauer's relation and, for soil and sand, with the parallel relation.

This proposed approach, grounded in commonly measured parameters, offers a practical method for predicting the thermal conductivity of moist porous insulation material. Its simplicity and reliance on readily available data enhance its feasibility for real-world implementation.

Further assessments for model improvement include combining the study with temperature-dependant thermal conductivity and evaluating the influence of material composition and microstructural characteristics to the models.

CRediT authorship contribution statement

C.H. Koh: Conceptualization, Methodology, Investigation, Formal analysis, Writing – original draft. **H.J.H. Brouwers:** Writing – review & editing, Supervision, Methodology, Investigation, Conceptualization.

Declaration of competing interest

The authors declare that they have no known competing financial interests or personal relationships that could have appeared to influence the work reported in this paper.

Data availability

Data will be made available on request.

References

[1] ISO, ISO 16957 Measurement of Apparent Thermal Conductivity of Wet Porous Building Materials By a Periodic Method, ISO, 2016.
[2] ISO, ISO 10051 Thermal insulation - moisture effects On Heat Transfer - determination of Thermal Transmissivity of a Moist Material, ISO, 1996.
[3] T. McFadden, Thermal Performance Degradation of Wet Insulations in Cold Regions, J. Cold Reg. Eng. 2 (1) (1988), https://doi.org/10.1061/(ASCE)0887-381X(1988)2:1(25).
[4] Y. Wang, C. Ma, Y. Liu, D. Wang, J. Liu, A model for the effective thermal conductivity of moist porous building materials based on fractal theory, Int. J. Heat. Mass Transf. 125 (2018) 387–399, https://doi.org/10.1016/j.ijheatmasstransfer.2018.04.063.
[5] X. Qin, J. Cai, P. Xu, S. Dai, Q. Gan, A fractal model of effective thermal conductivity for porous media with various liquid saturation, Int. J. Heat. Mass Transf. 128 (2019), https://doi.org/10.1016/j.ijheatmasstransfer.2018.09.072.
[6] W. Pei, F. Ming, M. Zhang, X. Wan, A thermal conductivity model for insulation materials considering the effect of moisture in cold regions, Cold. Reg. Sci. Technol. 207 (2023) 103770, https://doi.org/10.1016/j.coldregions.2022.103770.
[7] H. Li, Q. Zeng, S. Xu, Effect of pore shape on the thermal conductivity of partially saturated cement-based porous composites, Cement Concr. Compos. 81 (2017), https://doi.org/10.1016/j.cemconcomp.2017.05.002.
[8] Z. Chu, G. Zhou, R. Li, Enhanced fractal capillary bundle model for effective thermal conductivity of composite-porous geomaterials, Int. Commun. Hea Mass Transfer 113 (2020), https://doi.org/10.1016/j.icheatmasstransfer.2020.104527.
[9] Y. Chen, D. Li, X.-Q. Xie, Y. Gao, Y.-L. He, Theoretical modeling and experimental validation for the effective thermal conductivity of moist silica aerogel, Int. J. Heat. Mass Transf. 147 (2020), https://doi.org/10.1016/j.ijheatmasstransfer.2019.118842.
[10] B. Ghanbarian, H. Daigle, Thermal conductivity in porous media: percolation-based effective-medium approximation, Water. Resour. Res. 52 (1) (2015) 295–314, https://doi.org/10.1002/2015WR017236.
[11] J.K. Carson, S.J. Lovatt, D.J. Tanner, A.C. Cleland, Thermal conductivity bounds for isotropic, porous materials, Int. J. Heat. Mass Transf. 48 (11) (2005) 2150–2158, https://doi.org/10.1016/j.ijheatmasstransfer.2004.12.032.
[12] D.S. Smith, A. Alzina, J. Bourret, B. Nait-Ali, F. Pennec, N. Tessier-Doyen, K. Otsu, H. Matsubara, P. Elser, U.T. Gonzenbach, Thermal conductivity of porous materials, J Mater Res 28 (2013) 2260–2272, https://doi.org/10.1557/jmr.2013.179.
[13] A. Eucken, Allgemeine Gesetzmäßigkeiten für das Wärmeleitvermögen verschiedener Stoffarten und Aggregatzustände, Forschung auf dem Gebiet des Ingenieurwesens A 11 (1940) 6–20.
[14] Z. Hashin, S. Shtrikman, A Variational Approach to the Theory of the Effective Magnetic Permeability of Multiphase Materials, J. Appl. Phys. 33 (1962) 3125–3131, https://doi.org/10.1063/1.1728579.
[15] R. Landauer, The Electrical Resistance of Binary Metallic Mixtures, J. Appl. Phys. 23 (1952) 779–784, https://doi.org/10.1063/1.1702301.
[16] G. Tichá, W. Pabst, D.S. Smith, Predictive model for the thermal conductivity of porous materials with matrix-inclusion type microstructure, J. Mater. Sci. 40 (2005) 5045–5047, https://doi.org/10.1007/s10853-005-1818-x.
[17] J. Côté, J.-M. Konrad, A generalized thermal conductivity model for soils and construction materials, Canad. Geotech. J. 42 (2) (2005) 443–458, https://doi.org/10.1139/t04-106.
[18] J.M. Markle, R.A. Schincariol, J.H. Sass, J.W. Molson, Characterizing the Two-Dimensional Thermal Conductivity Distribution in a Sand and Gravel Aquifer, Soil Sci. Soc. Am. 70 (4) (2006) 1281–1294, https://doi.org/10.2136/sssaj2005.0293.
[19] Y. Lin, Z. Shi, P.L. Wildfong, Thermal conductivity measurements for small molecule organic solid materials using modulated differential scanning calorimetry (MDSC) and data corrections for sample porosity, J. Pharm. Biomed. Anal. 51 (4) (2010) 979–984, https://doi.org/10.1016/j.jpba.2009.10.022.
[20] Y. Çengel, J. Cimbala, Appendix 1 Property tables and charts. Fluid Mechanics Fundamentals and Applications, McGraw Hill, 2006.
[21] Fraunhofer-IBP, "MASEA Datenbank," 2024. [Online]. Available: https://www.masea-ensan.de/.
[22] M. Jiřičková, Z. Pavlík, L. Fiala, R. Černý, Thermal Conductivity of Mineral Wool Materials Partially Saturated by Water, Int. J. Thermophys. 27 (4) (2006) 1214–1227, https://doi.org/10.1007/s10765-006-0076-8.
[23] C. Clauser, E. Huenges, Thermal Conductivity of Rocks and Minerals, Rock Phys Phase Relat Handbook Phys. Const. 3 (1995), https://doi.org/10.1029/RF003p0105.
[24] Y. Yang, Thermal Conductivity," in *Physical Properties of Polymers Handbook*, Springer, 2007, pp. 155–164.
[25] M. Antlauf, N. Boulanger, L. Berglund, K. Oksman, O. Andersson, Thermal Conductivity of Cellulose Fibers in Different Size Scales and Densities, Biomacromolecules. 22 (2021) 3800–3809, https://doi.org/10.1021/acs.biomac.1c00643.
[26] H. He, K. Noborio, Ø. Johansen, M.F. Dyck, J. Lv, Normalized concept for modelling effective soil thermal conductivity from dryness to saturation, Eur. J. Soil. Sci. 71 (1) (2019), https://doi.org/10.1111/ejss.12820.
[27] D. Taoukil, A.E. bouardi, F. Sick, A. Mimet, H. Ezbakhe, T. Ajzoul, Moisture content influence on the thermal conductivity and diffusivity of wood–concrete composite, Constr. Build. Mater. 48 (2013), https://doi.org/10.1016/j.conbuildmat.2013.06.067.
[28] A. Bouguerra, Prediction of effective thermal conductivity of moist wood concrete, J. Phys. D. Appl. Phys. 32 (1999), https://doi.org/10.1088/0022-3727/32/12/318.

[29] H. He, M. Li, M. Dyck, B. Si, J. Wang, J. Lv, Modelling of soil solid thermal conductivity, Int. Commun. Heat Mass Transfer 116 (2020) 104602, https://doi.org/10.1016/j.icheatmasstransfer.2020.104602.
[30] W.H. Somerton, J.A. Keese, S.L. Chu, Thermal Behaviour of Unconsolidated Oil Sands, SPEJ (1974) 513–521.
[31] K. Udell, J.S. Fitch, Heat and Mass Transfer in Capillary Porous Media Considering Evaporation, Condensation and Non-Condensible Gas Effects, in: 23rd ASME/AIChE national heat transfer conference, 1985, pp. 103–110.
[32] WUFI, WUFI Material (North America and Fraunhofer-IBP Databases), WUFI, 2024.